The 17th Spacecraft Charging Technology Conference, Palais des Papes, Avignon, France, June 17-21, 2024

Internal Charging Analysis of Floating Metallic Parts with FASTRAD.

J.M. Plewa[1], M. Sevoz[2], A. Samaras[2], F. Fontanel[2] and R. Mangeret[2]
[1]TRAD Tests & Radiations, Labège, France
[2]AIRBUS Defence & Space, Toulouse, France

***Abstract*— High-energy electrons from space environment can penetrate through the spacecraft and charge sensitive elements located inside. The build-up of electric charges that can lead to an electrostatic discharge mainly occurs at the boundary between dielectrics and floating metals. The internal charging module of FASTRAD was improved to compute the increase in potential of floating metals and stored energy of charged dielectrics. We focus on two typical cases that illustrate how to treat floating parts in the frame of an internal charging analysis. The first case is about a floating coaxial cable between two radio frequency switching modules. The cable conductor, if unterminated at both ends, can store high levels of charge that can be suddenly released into the payload components at the commutation of the switches. The energy level stored in the cable is estimated. We also compare the 1D and 3D analysis to quantitively show how much the margins can be decreased by using the 3D geometry. The second case is about a floating metallic cover on an electronic component mounted on a PCB inside an equipment. This floating cover can be either below or above a layer of a conformal coating. The potential and electric field are computed for both situations and we show that the cover can no longer be considered as an ESD risk, so allowing grounding requirements relaxation, in case it is fully embedded below a layer of conformal coating. Again, 1D and 3D analysis are compared in order to refine margins and allow relevant relaxation on grounding generic requirements, securing also the double isolation requirements.**

***Index Terms*—Internal charging, dielectrics, floating metallic parts, 3D calculations, Monte Carlo particle transport, finite element analysis.**

I. Introduction

Internal charging of dielectrics or floating metallic parts in spacecraft is a well-known risk for space missions where high energy electron flux are intense. Standards give recommendations to avoid electrostatic discharges (ESD) as soon as the design phase. However, some specific situations require to go further in the internal charging analysis to better assess the ESD risk.

In this work, we present two specific situations where a 3D internal charging analysis is carried out with FASTRAD to better understand the charging of floating metallic parts. The first case is about a floating coaxial cable between two radio frequency switching modules and the second case is about a floating metallic cover on an electronic component mounted on a PCB inside an equipment. In each case, the 3D results are compared to 1D results and they are discussed.

II. Radiation environment

The space radiation environment used for this study was computed with the FLUMIC model [1] by using a GEO orbit in the DICTAT tool [2] from SPENVIS [3]. A daily averaged worst-case was computed (**Fig. 1**).

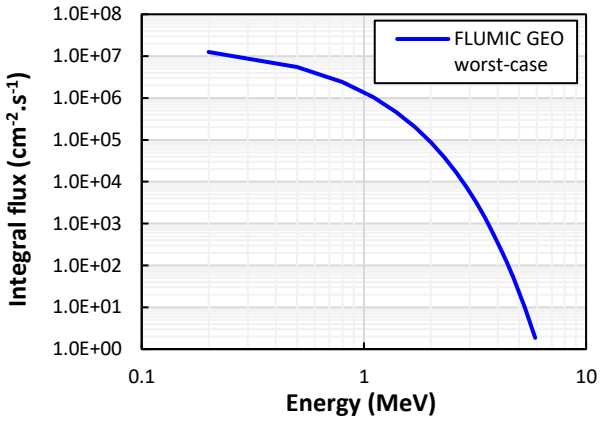

Fig. 1. FLUMIC daily averaged GEO worst-case.

III. Floating coaxial cable

A. *Modelling*

A detailed 3D radiation model of a telecommunication spacecraft in GEO orbit is used (**Fig. 2**). Two electronic units representing the radio frequency switching modules are placed outside the spacecraft just below an MLI (**Fig. 3**). A simple coaxial cable is located between the two units. This geometry setup allows us to represent the shielding surrounding the cable of a realistic case. It is worth noting that these equipments and coaxial cable are usually mounted underneath multilayers thermal blankets, providing additional shielding to the charging environment, and not taken into account in the simulations as a worst-case situation.

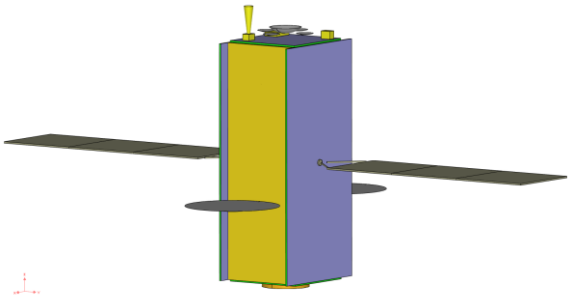

Fig. 2. Radiation model of the spacecraft. The height is 3 meters. Units are under the MLI (yellow side).

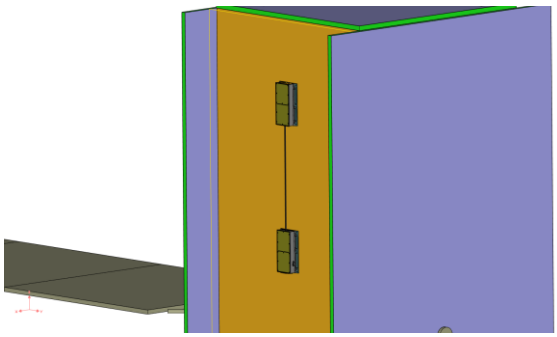

Fig. 3. Two units are located under an MLI (hidden here) and there is the studied coaxial cable between them.

The cable reference is MCJ205A and the length is 50 cm in this example. A cross-section of the cable is displayed in **Fig. 4**. The materials and densities are given in TABLE I.

For the calculation of the charge build up in the various layers, the center conductor is left floated (not grounded), whereas outer and inner shields are grounded to the spacecraft structure. Other layers (PTFE, Tefzel®, Aracon®) are dielectrics

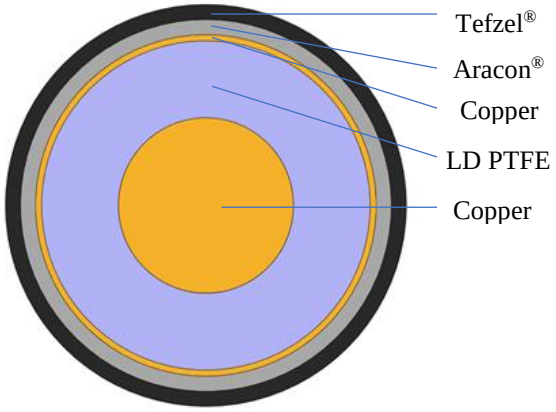

Fig. 4. Cross-section of the cable. The spacecraft panel -X is below the cable.

TABLE I
MATERIAL DESCRIPTION OF THE CABLE.

Name	Material	Density (g/cm^3)
Center Conductor	Copper	8.96
Dielectric	Low Density PTFE	0.75
Inner Shield	Copper	8.96
Outer Shield	Aracon®	1.44
Jacket	Tefzel®	1.70

B. *Monte Carlo particle transport*

The charge deposition rate is scored in a 3D volume mesh. To get a smooth 3D map in a reasonable calculation time, a Reverse Monte Carlo particle transport was done and only for a 1 cm length section of the cable. The charge deposition rate is only scored for the dielectric and for the center floating conductor. There are 36,420 sub-volumes making up the 3D map. A cross-section of the charge deposition rate of the primary electrons is displayed in **Fig. 5**. The charge deposition rate is ranging from -3.1×10^{-11} C/m^3/s to -1.6×10^{-6} C/m^3/s. The highest value of the charge rate is at the top boundary dielectric/conductor due to the scattering of the electrons and the high density of the copper compare to the dielectric. The top side is the most exposed area while the bottom of the cable is more protected. A 1D radial profile of the charge deposition rate at the center of the cable is given in **Fig. 6**. The two pics at -1.5 mm and +1.5 mm are due to the scattering of electrons at the boundary with the metallic conductor.

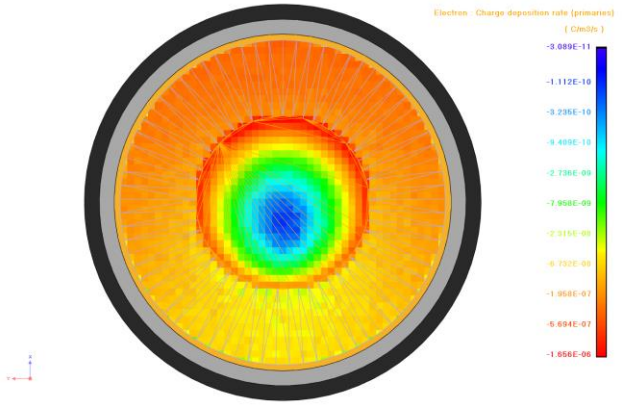

Fig. 5. Cross-section of the charge deposition rate inside the dielectric and the conductor. The color scale is logarithmic.

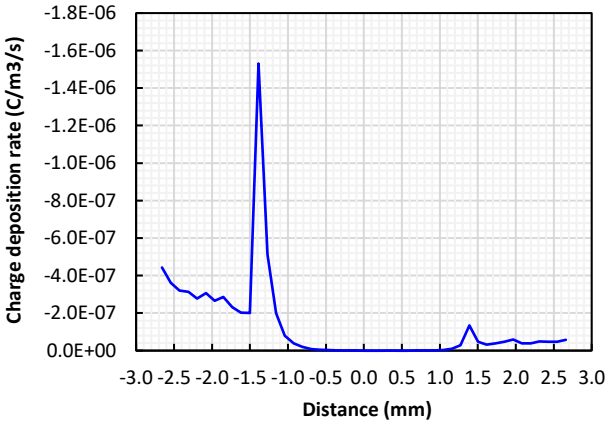

Fig. 6. Radial profile of the charge deposition rate in the cable.

C. *Finite element analysis*

A time dependent modelling is carried out to compute the slow conduction of the embedded charges, by using the charge conservation law with a volume source term $\dot{\rho}$ expressed in $C/m^3/s$, the Ohm's law and the Maxwell-Gauss's equation. Combining these equations leads to the differential equation (1) where the variable ϕ is the potential expressed in V, σ is the total bulk conductivity expressed in $\Omega^{-1}.m^{-1}$ and ε is the permittivity expressed in F/m.

$$-\nabla\varepsilon\nabla\frac{\partial\phi}{\partial t} - \nabla\sigma\nabla\phi = \dot{\rho} \quad (1)$$

Equation (1) is solved in 3D by FASTRAD by using the finite element method. This feature is available in the internal charging module. More details about this module are given in the proceedings of the SCTC 2022 [4].

For the 3D potential and electric field calculations, only the dielectric and the center conductor are considered. As the inner and outer shields of the cable are grounded it is not needed to simulate the external layers above the dielectric, a boundary condition is enough. The outer boundary of the dielectric is simply grounded by assigning a 0 V potential. The center conductor is floating i.e. no boundary condition is assigned so that the potential can build up. The 1 cm length section of the cable is meshed with a very fine unstructured tetrahedral volume mesh. It consists of 2.77×10^6 of tetrahedrons to get smooth maps of potential and electric field.

The relative permittivity of the dielectric is $\varepsilon_r = 2.15$ and the bulk conductivity is $\sigma_0 = 6\times10^{-16}$ $\Omega^{-1}.m^{-1}$. From these material parameters the time constant is about $\tau \approx 9$ h. The conduction calculation is run until the steady state is reached i.e. up to 48 h ($5\,\tau \approx 44$ h).

Fig. 7 to **Fig. 10** displays the potential and the electric field at the steady state. The center conductor is represented in wireframe and the dielectric is hidden. The maximum potential reached is -358 V. The potential gradient is the highest for the top side because it is more irradiated (**Fig. 7**). This variation is given by the electric field (**Fig. 9**) where the maximum value is 0.50 MV/m. Radial profiles of the potential and electric field are displayed in **Fig. 8** and **Fig. 10** respectively.

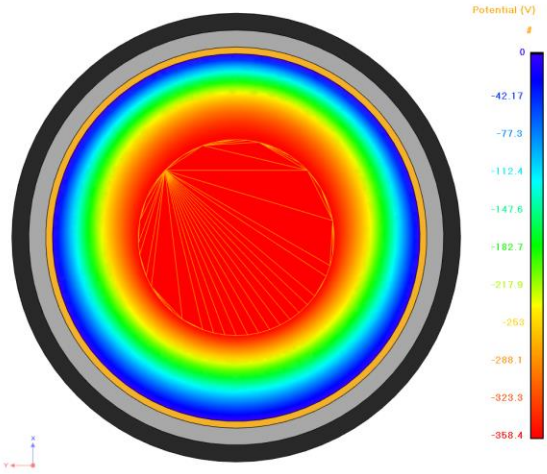

Fig. 7. Cross-section of the potential inside the cable at steady state.

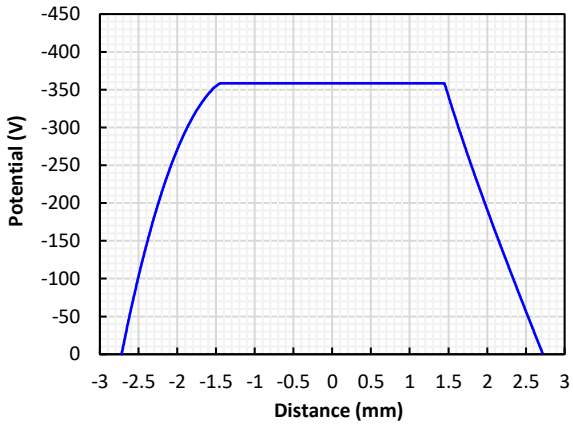

Fig. 8. Radial profile of the potential.

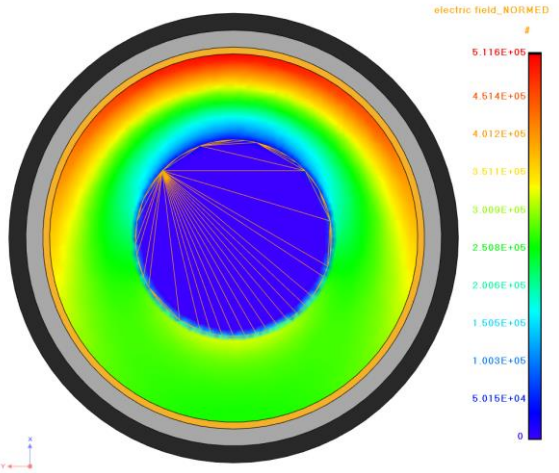

Fig. 9. Cross-section of the electric field inside the cable at steady state.

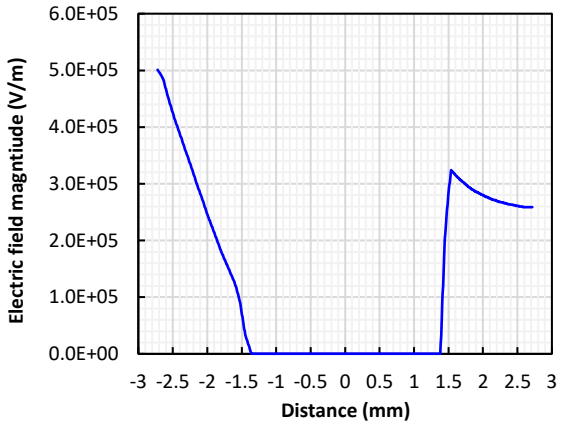

Fig. 10. Radial profile of the electric field.

The highest value of the electric field 0.50 MV/m is lower than the dielectric strength of the material, and also lower than the ECSS ESD standard [5] (E < 10 MV/m) therefore no electric breakdown through the dielectric is expected. However, the discharge energy level released during the commutation toward the radio frequency equipment input should be carefully assessed as a risk.

New features have been added in FASTRAD in order to compute the capacitance C and the stored electric energy E of the coaxial cable at the steady state. At the end of the conduction calculations, these quantities are computed for the dielectric by FASTRAD with the finite element analysis (FEA). From the results obtained for 1 cm length, the capacitance and the stored energy are inferred for the full-length cable (50 cm) leading to C = 95.1 pF and E = 6.1 µJ. These values were checked with the analytical solutions for a cylindrical capacitor, equations (2) and (3), leading to a difference of 0.1% for the capacitance et 0.3 % for the energy. The capacitance and the stored energy are very useful inputs for an electromagnetic compatibility analysis at the system level with other tools.

$$C = \frac{2\pi\varepsilon_0\varepsilon_r l}{ln\left(\frac{R_{ext}}{R_{int}}\right)} \quad (2)$$

$$E = \frac{1}{2}CU^2 \quad (3)$$

D. *Comparison to 1D methods*

The simple internal charging analysis given in the NASA handbook 4002B [6] was used to get the potential and the electric field in the dielectric. The geometry is not anymore cylindrical but simplified in layers of materials. This method relies on the CSDA (continuous slow down approximation) range of electrons through aluminum to get the exit current of each layer and estimate the deposited current in the dielectric and therefore the potential and the electric field. With this method, the maximum potential is -2330 V and the maximum electric field is 1.83 MV/m.

Then the DICTAT tool [7] was run by using the cylindrical geometry. Three thicknesses can be modelled: one for the dielectric, one for the shielding and one for the conductor. The different materials surrounding the dielectric are modelled by one equivalent aluminum thickness. The maximum potential is -743 V and the maximum electric field is 1.02 MV/m.

Comparison of these 1D results to the 3D results obtained with FASTRAD are summarized in TABLE II. There is a factor about 2, for both potential and electric field with DICTAT. With the NASA handbook method, we get a factor 6.5 and 3.7 for potential and electric field respectively.

TABLE II
COMPARISON BETWEEN 3D AND 1D RESULTS.
RATIO IS GIVEN WITH RESPECT TO FASTRAD.

Type	Potential (V)	Ratio	E. Field (MV/m)	Ratio
FASTRAD (3D)	-358	1	0.50	1
DICTAT (1D)	-743	2.1	1.02	2.0
NASA-HDBK (1D)	-2330	6.5	1.83	3.7

If the values of potential obtained with the 1D methods are used to get the stored energy from the analytical equation (3), the difference with FASTRAD is squared since the potential is squared. Therefore, a factor 4 and 42 for the stored energy are found by using the potential from DICTAT and from the NASA handbook method respectively.

The 1D methods remain very helpful to identify the parts or the area where an IESD risk is likely. They are complementary of 3D methods which are time consuming and are made to focus on one object. However, when the margins must be reduced as much as possible, when a complex geometry is used or when an anomaly must be studied in a much less conservative manner, we show that 3D methods use is required for more realistic assessment.

IV. Floating Metallic Cover

A. *Modelling*

The same spacecraft model is used as for the previous analysis (**Fig. 11**). An electronic unit is located inside the spacecraft (**Fig. 12a**) along with a coated FP16 component inside the unit (**Fig. 12b**). The metallic cover of the component is floating and made of tantalum oxide, to ensure a shielding role against space radiations. The box is made of alumina and the leads are made of Kovar®. The material properties are given in TABLE III. The coating displayed in wireframe in the **Fig. 12b** is 200 µm thick and made of epoxy resin.

TABLE III
Material Description Of The FP16 Component.

Name	Material	Density (g/cm^3)	Relative permittivity	Conductivity (S/m)
Floating cover	Tantalum oxide	6.00	-	10^6
Box	Alumina	3.97	9.0	10^{-16}
Conformal coating	Epoxy resin	1.50	3.6	10^{-16}
Leads	Kovar®	8.36	-	10^6

Two cases are studied in this part: the floating metallic cover (i) below and (ii) above the conformal coating. A Monte Carlo particle transport was carried out for both situations as well as a finite element analysis to get the potential and the electric field.

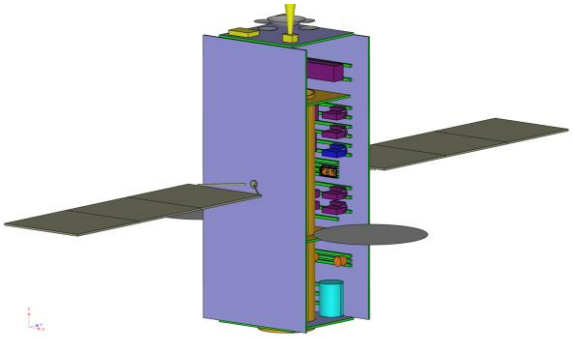

Fig. 11. Spacecraft model overview.

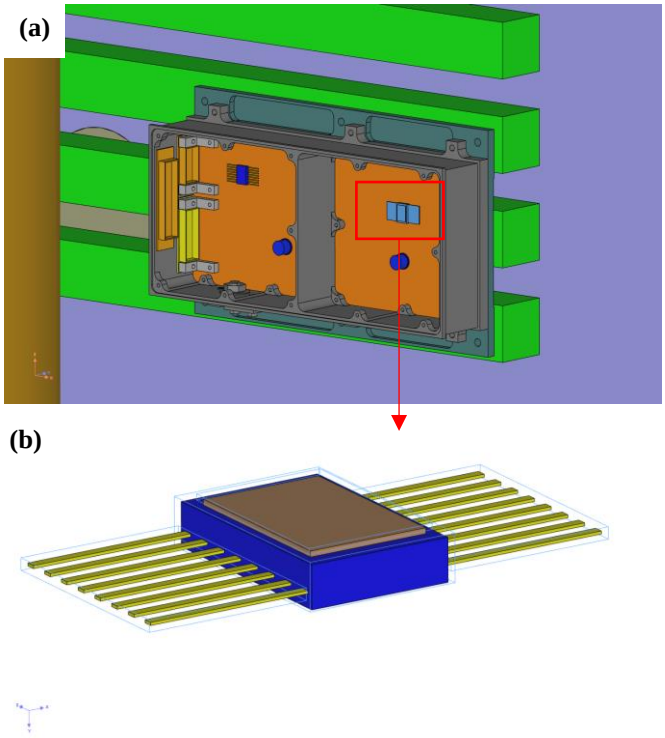

Fig. 12. (a) Unit inside the spacecraft. The top cover of the unit housing is hidden to see inside. (b) Studied electronic component; FP16 box with the conformal coating displayed in wireframe.

B. *Monte Carlo particle transport*

A Reverse Monte Carlo particle transport was run on the FP16 component by using the same space radiation environment as for the previous analysis i.e. a daily averaged integral flux for a GEO worst-case (**Fig. 1**). A 3D map of the charge deposition rate of the primary electrons was carried out for both cases, with about 2×10^5 sub-volumes (**Fig. 13** and **Fig. 14**). The maximum charge rates are -1.07×10^{-7} $C/m^3/s$ and -6.54×10^{-8} $C/m^3/s$ for the cover below and above the conformal coating respectively. The same color scale is used in **Fig. 13** and **Fig. 14** to highlight the differences, however small. These 3D charge rates are used as source term for the quasi-electrostatic conduction calculations.

It is worth noting that the Radiation Induced Conductivity (RIC) characteristics are not considered for the simulations (conservative).

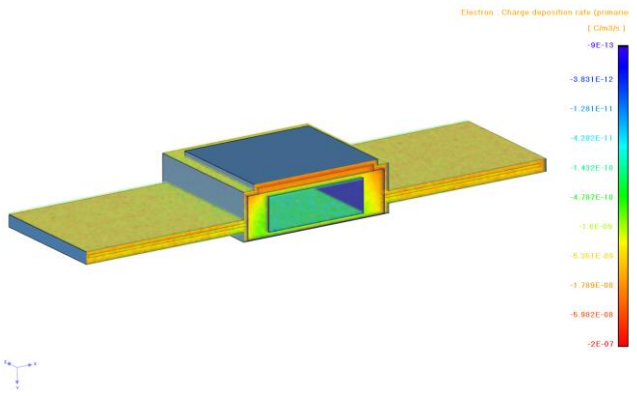

Fig. 13. 3D maps of the charge deposition rate inside the component with the cover **below** the conformal coating.

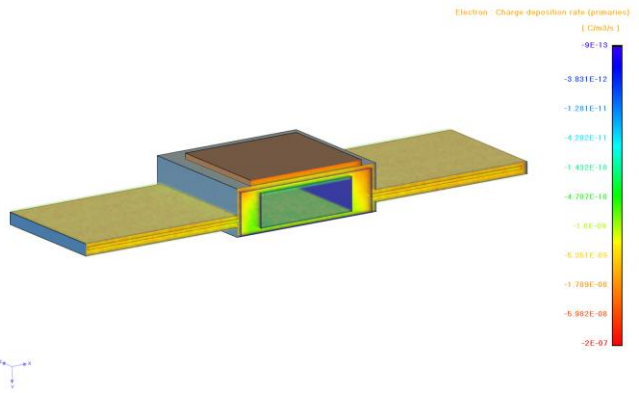

Fig. 14. 3D maps of the charge deposition rate inside the component with the cover **above** the conformal coating. The same color scale is used with the previous configuration ***below***.

C. *Finite element analysis*

In both cases, the metallic cover is floating. One pin is grounded (0 V) and two other pins are set to +12 V and -12V as displayed in **Fig. 15**.

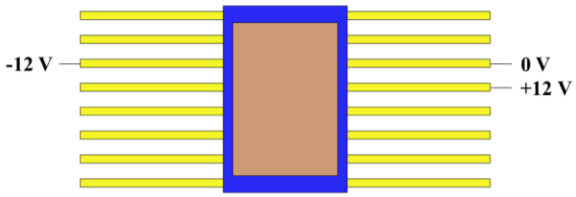

Fig. 15. Boundary conditions for the potential. Metallic parts with no boundary conditions are floating.

The FASTRAD results are summarized in TABLE IV. The minimum and maximum potentials are given for the whole component along with the potential reached by the metallic cover. The maximum electric field is given for the dielectric surrounding the cover.

TABLE IV
FASTRAD RESULTS

Cover location	Min. Potential (V)	Cover Potential (V)	Max. Potential (V)	Max. Electric Field (V/m)
Below coating	-597.5	-681.7	-787.7	1.865×10^5
Above coating	-493.5	-587.3	-722.2	2.992×10^5

The maps of potential and electric field reached at the steady state are displayed in **Fig. 16**.

When the cover is below the conformal coating, it reaches a slightly higher potential than when it is placed above due to charge deposition inside the coating above the cover.

However, the electric field inside the dielectric near the cover is lower when the cover is below the conformal coating. The highest value of the electric field 0.3 MV/m is lower than the dielectric strength of the material, and also lower than the ECSS ESD standard (E<10MV/m) therefore no punch through/ electric breakdown through the dielectric is expected.

When the cover is above the conformal coating, the maximum electric field in the dielectrics surrounding the metallic cover is increased by 60%. In this case, the electric field is also increased due to the sharp corner of the cover.

The potential difference is low when the cover is below the conformal coating therefore the ESD risk is low too. Furthermore, in this configuration there is no triple junction (i.e. interface between vacuum, dielectric and metal) that could initiate an ESD as is the case in the second configuration where the cover is placed above the conformal coating. This example confirms that when the floating metallic cover is below a conformal coating, it may no longer be considered as floating and is also not required to be grounded.

This has also the advantage to avoid delicate grounding operations which could violate the double insulation constraints.

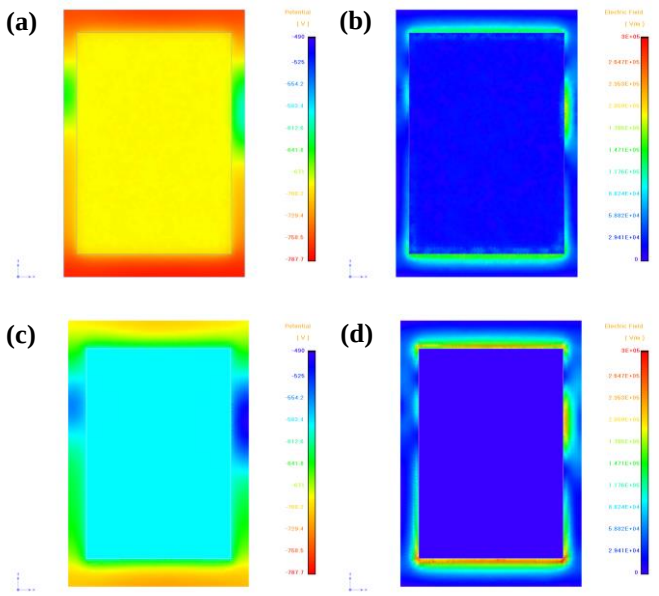

Fig. 16. Top views of the FP16 component. (a) and (c) 3D maps of the potential at steady state. (b) and (d) 3D maps of the electric field at steady state. (a) and (b) the cover is below the conformal coating. (c) and (d) the cover is above the conformal coating. The same color scale is used for each quantity. Min. and max. values are given in TABLE IV.

D. *Comparison to 1D methods*

The shielding and the FP16 geometry are simplified into layers of each material: the shielding, the coating, the cover and the box (**Fig. 17**).

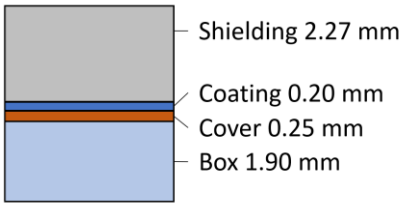

Fig. 17. Simplification of the geometry for the 1D calculations.

A sector-based analysis (ray-tracing) was carried out with FASTRAD to get the shielding surrounding the component. The minimum thickness was used (2.27 mm). The configuration of the cover, below or above the conformal coating, is not important since in the 1D calculations the layers above the dielectric are considered as aluminum equivalent thicknesses. The bottom of the dielectric is grounded.

The results of the 1D calculations are displayed in the TABLE V. The potential and the electric field are given for the dielectric at the equilibrium state. The electric field is about 0.07 MV/m and 2.11 MV/m given by DICTAT and the NASA handbook method respectively. The difference between theses two results can be explained by the fact that in DICTAT the inner face of the dielectric was grounded which allows to decrease the potential while in the NASA handbook method only the potential is only estimated from the current trapped inside the dielectric layer.

TABLE V
1D RESULTS.

Type	Potential (V)	E. Field (MV/m)
DICTAT (1D)	-105	0.07
NASA-HDBK (1D)	-4002	2.11

In the previous section, the 3D results given by FASTRAD displayed in TABLE IV are greater than DICTAT and lower than the NASA handbook method. It shows that complex geometry and ground configuration are difficult to simplify for 1D calculations, which can underestimate or overestimate results. Especially in this case where the charging of the floating metallic cover has a significant impact on the potential and it is not taken into account in 1D calculations where it is only considered as a shielding.

V. CONCLUSION

The FASTRAD internal charging module has been improved by the addition of the calculation of the capacitance and the stored energy of floating coaxial cables. In this work, we validate the results from the FEA with an analytical calculation. Therefore, after the internal charging analysis with FASTRAD, these quantities can be the inputs for a risk analysis or an electromagnetic compatibility analysis at the system level with other tools (electrical circuits solver).

The 1D methods remain very helpful to identify the parts or the area where an IESD risk is likely and they are a first order of magnitude assessment of charging hazards, with risk of underestimation in some cases. However, when the margins must be reduced as much as possible, we show that 3D methods can play a significant role in offering optimization in design, accommodation and grounding rules elaboration, during a new platform development, or in supporting complex investigations related to anomalies.

The comparison of the charging of a component with a metallic cover below or above a conformal coating was carried out. We found that the potential difference is low when the cover is below the conformal coating and the electric field was decreased by 60%, therefore mitigating the ESD risk. This example confirms, as also suggested by ECSS-E-ST-20-06C [5] that when the floating metallic cover is below a conformal coating, it may no longer be considered as floating, and will not require delicate grounding operations during the PCB manufacturing.

VI. REFERENCES

[1] D. Rodgers, K. Hunter and G. Wren, "The FLUMIC Electron Environment Model," *8th Spacecraft Charging Technology Conference*, 20-24 october 2004.

[2] D. Rodgers, K. Ryden, G. Wrenn, P. Latham, J. Sorensen and L. Levy, "An Engineering Tool for the Prediction of Internal Dielectric Charging," *6th Spacecraft Charging Technology Conference*, 2000.

[3] BIRA-IASB, "SPENVIS website (ESA's SPace ENVironment Information System)," [Online]. Available: https://www.spenvis.oma.be/.

[4] J.-M. Plewa, M.-C. Ursule, L. Sarie, A. Varotsou, A. Samaras, F. Fontanel, M. Sevoz and R. Mangeret, "3D Internal Charging Analysis with FASTRAD," *Proceedings of Spacecraft Charging Technology Conference*, 2022.

[5] ECSS-E-ST-20-06C_Rev1, 2019.

[6] NASA-HDBK-4002B, 2022.

[7] "DICTAT (Dielectric Internal Charging Threat Assessment Tool)," [Online]. Available: https://www.spenvis.oma.be. [Accessed 11 03 2020].